Manuscript title: Numerical techniques for fast generation of discrete-element models of large soil volumes

Authors: Matteo O. Ciantia[1], Katia Boschi[2], Thomas Shire[3] and Sacha Emam[4]

Affiliations: [1]School of Science and Engineering, University of Dundee, UK; [2]Dept. Civil and Environmental Engineering, Politecnico di Milano, Italy; [3]Dept. Civil and Environmental Engineering, University of Glasgow, UK and [4]Itasca consultants, Lyon, France

Corresponding author: Matteo O. Ciantia, School of Science and Engineering, University of Dundee, Dundee, UK. Tel.: +447481910815.

E-mail: m.o.ciantia@dundee.ac.uk

Abstract

In recent years, civil engineers have started to use discrete-element modelling to simulate large-scale soil volumes thanks to technological improvements in both hardware and software. However, existing procedures to prepare ‘representative elementary volumes’ are unsatisfactory in terms of computational cost and sample homogeneity. In this work, a simple but efficient procedure to initialise large-scale discrete-element models is presented. Periodic cells are first generated with a sufficient number of particles (enough to consider the cell a representative elementary volume) matching the desired particle size distribution and equilibrated at the desired stress state, porosity and coordination number. When the cell is in equilibrium, it is replicated in space to fill the problem domain. And when the model is filled, only a small number of mechanical cycles is needed to equilibrate a large domain. The result is an equilibrated homogeneous sample at the desired initial state in a large volume.

Keywords: Geotechnical engineering; Granular materials; Computational mechanics; Models (physical), DEM

1. Introduction

The discrete-element method (DEM), first proposed by Cundall and Strack (1979), is a numerical approach widely used to study fundamental aspects of soil response (Calvetti et al., 2003; Huang et al., 2014b; Ciantia et al., 2016b, 2018). Typically, small cubic or cylindrical samples are generated to obtain a 'representative elementary volume' (REV), which is later tested to explore different links between micromechanical features and the mesomechanical response of soil. Element tests may be simulated by adopting boundaries that mimic conditions typical of physical soil tests. These include rigid walls (Tamagnini et al., 2005; Calvetti, 2008; Ciantia et al., 2015, 2016b), flexible membranes (Kuhn, 1995; Cheung and O'Sullivan, 2008) and periodic boundaries (Thornton, 2000; Esnault and Roux, 2013). This latter has the advantage of eliminating boundary-effects (e.g. Thornton and Zhang, 2010) which are known to influence the material response (Huang et al., 2014a).

The mechanical response of granular media is strongly dependant on the initial state of the material. In particular, stress and porosity at the mesoscopic level and coordination number (Z) at the microscale (Roux, 2004; Agnolin and Roux, 2007a). Hence attaining a specified initial state for a given particle size distribution (PSD) is a crucial step of DEM modelling in soil mechanics. Different procedures have been tried and tested with some success to create REVs suitable for element testing. Those used more often include the radius expansion method (REM) (Cundall and Strack, 1979; Rothenburg and Bathurst, 1992), the fixed point method (Katsuki et al., 1989), the isotropic compression method (Cundall and Strack, 1979), the modified isotropic compression method (Thornton, 2000) and the multi-layer under compaction method (Jiang et al., 2003). These procedures pose important problems when the method is used to initialise engineering scale geotechnical problems. Indeed, when the model dimension to particle size ratio becomes large, the computational cost of system initialisation quickly becomes prohibitive. Moreover, specimen homogeneity is difficult to attain (Butlanska et al., 2014; Ciantia et al., 2014).

In this paper, building on the preliminary studies of Ciantia et al. (2017) and Ciantia and Shire (2017), a simple but efficient procedure to initialise large-scale DEM models is presented: the periodic cell replication method (PCRM). Small samples are first generated under zero gravity with a sufficient number of particles (enough to consider the cell as a REV) by matching a desired PSD and using periodic boundaries. These are then equilibrated at the desired stress, porosity and coordination number. Once the cell is in equilibrium, by exploiting the periodic characteristic of the sample, it is replicated in space to fill the whole model domain. If the boundary conditions of the large model are still periodic, no gravity is considered and the stress state imposed is uniform and equivalent to the original cell, just a few mechanical cycles are needed to re-equilibrate the large domain. The result is a large homogeneous sample, equilibrated under a prescribed stress at the desired porosity.
In the first part of this paper it is shown that the PCRM can hence be used to speed up REV sample generation. On the other hand, as both zero-gravity and periodic boundaries do not appear naturally in the definition of most engineering-scale boundary value problems (BVPs), the PCRM alone is found to be unsuitable for the initialisation of BVP samples. In the second part of the paper, novel numerical techniques that enable the use of the PCRM to initialise large-scale DEM models under gravity conditions and in the presence of rigid walls are presented. In particular, to achieve equilibrated and homogenous samples, features such as contact force (CF) scaling and contact overlap modification are employed to minimize the

effect of using rigid wall boundary conditions of the BVP. CF scaling and contact gap modification are also fundamental features used to prescribe non-uniform stress states such as typical field and small scale BVP experimental stress conditions (including centrifuge experiments) where the principal directions are vertical and horizontal and the effective horizontal stress is proportional to the effective vertical one (hence k where $k=\sigma'_h/\sigma'_v$). Finally, it is shown that for BVPs such as a cylindrical calibration chamber, REV samples characterised by a rigid cylindrical wall in the radial direction and periodic boundary conditions in the cylinder axis direction make sample preparation 17 times faster than the classic pluviation technique. In this work efficiency will be represented by model runtime as all the simulations were performed using the same hardware (Intel Xeon CPU E5 2680 v4 @2.4GHz with 32GB of Ram) and software, PFC3D (Itasca, 2017).

2. The periodic cell replication method (PCRM)

2.1. Sample preparation and initial conditions

A small (*S*), medium (*M*) and large (*L*) cubical discrete specimens with 1.5, 3, 6 mm side (corresponding to about 1,500, 5,000 and 40,000 particles respectively) in periodic space were created using the Radius Expansion Method (REM). Particle sizes were selected to match the weight cumulative PSD of Fontainebleau sand (FS). Following the REM, velocities were set to zero. Isotropic compression to an initial mean normal stress (p_0') of 10 *kPa* with an interparticle friction coefficient (μ) selected by trial and error was used to generate a sample with a close fit to the target initial porosity (n_0) of 0.39. n_0 was selected in order to numerically reproduce an experimental triaxial compression test on FS performed by El Dine et al. (2010). The average internal porosity was monitored through a measurement sphere (MS) centred in the centre of the cubic sample in exam and with a diameter equal to 0.8 times the minimum sample length. The total porosity of the sample was also measured by considering the whole sample size. To highlight the strong influence of coordination number (Z) on the REV mechanical response, a second small sample (*S**), characterised by the same n_0 and p_0' of *S* but with a higher initial Z (Z_0), was also prepared. This was done by starting form a slightly lower initial porosity during the particle random generation stage and applying longer cycle intervals with $\mu = 0$ during the compaction stage. Table 1 summarises the DEM model characteristics at the end of the generation phase. In order to capture the rotational resistance that exists between real non-spherical irregular grains, instead of using a moment resisting contact law, the DEM spherical particle rotation is inhibited (Ting et al., 1989; Calvetti, 2008; Ciantia et al., 2014). In this work, the simplified Hertz–Mindlin contact law is used along with the standard DEM formulation (Itasca, 2017). Table 2 reports the calibrated contact model parameters while Figure 1 represents the initial state of the *S*, *M* and *L* DEM samples. Triaxial compression tests on 100 *kPa* isotropically confined samples were then performed and the results are shown in Figure 2 where experimental trends are also reported. To perform a quasi-static test, during the shearing stage a strain rate was employed such that the inertial number was always maintained less than 10^{-3}. The large fluctuations clearly visible for the *S* sample reduce as the cell size and particle number increase. It can also be observed that the *S** sample, despite having the same n_0, has a much stiffer response when compared to the *S* sample. This result is in line with the observations of Agnolin and Roux (2007b) in that the response of the sample with higher Z_0 is stiffer despite n_0 and p_0' being equivalent. As the response of the *S* sample is very unstable, depending on the application either the *M* or the *L* models, which show a smoother response, can be selected as REVs. When using the DEM a REV may be defined as a model whose mechanical response is independent of the sample size and type of boundaries used (rigid or periodic). There are

no clear indications in the literature that define what is the minimum sized REV. According to the authors being the size of an REV strongly dependent on the PSD the trial and error technique is the only and safest approach that should be used. As reported in Table 1 the equilibrated initial state for the *S*, *M* and *L* samples was obtained after 4, 31 and 160 minutes respectively.

2.2. REV from PCRM

To exploit the idea of the PCRM, the equilibrated *S* and *M* samples were replicated in space to fill cubic cells with the size of the *L* sample. The *S* sample was hence replicated 27 time while sample *M* was replicated 8 times. In this way two large cell replicated samples (*L-CRS*) were generated: *L-CRS(S)* made from 27 *S* cells and *L-CRS(M)* made from 8 *M* cells. Both samples now have the same number of particles of an *L* sample but they were made starting from a non-REV and an REV cell respectively. The main characteristics of *L-CRS(S)* and *L-CRS(M)* are summarised in Table 3. The slight differences between the internal and total values of both initial porosity and coordination number in Table 1 represent the level of non-homogeneity of the unit cells used. Upon replication the total values remain unchanged while the internal ones get closer to the total ones (Table 3). For an ideal perfectly homogenous sample the internal and total values would coincide and remain unchanged upon replication. The same triaxial compression test was then performed on these two new samples and the results are shown in Figure 3. Although one may expect the *L-CRS(S)* sample, now made up 40,000 particles, to behave as a REV, this does not occur. The model does lose the local fluctuations but inherits a smoothed general trend of the *S* sample as a sort of best line fit. On the other hand, the *L-CRS(M)* which was generated from a REV (sample *M*) continues to behave as a REV. The time needed to generate these samples in an equilibrated condition from replicas resulted to be 8 minutes. If we add the time required to prepare the *S* and *M* cells, it results that a *L* sample can be obtained in 12 and 37 minutes respectively. This corresponds to 7.5% and 23% of the time spent with the standard procedure (160 minutes). As it would be highly efficient to prepare a large DEM sample starting from a non-REV cell (sample *S*), a parametric analysis testing a procedure aimed at disturbing the *L-CRS(S)* to obtain a REV was performed. The diameter of each particle was randomly multiplied by a factor between $1\pm\Delta D$ and re-equilibrated before the compression phase. As reported by Ciantia and Shire (2017), diameter expansion coefficients ΔD of 0.1% and 0.0001% were not sufficient to disrupt the cell replicated sample (CRS) inherited behaviour while, as represented in Figure 4, a factor of $\Delta D = 0.75\%$ is sufficient to disrupt this periodic inherited behaviour without changing the PSD. However, the re-equilibration following the diameter modification required 60 minutes, making the procedure less efficient than the one using the *M* sample as initial unit cell. An alternative method in which a small (0.01 m/s) random initial velocity (v_{ini}) was assigned to each particle and the sample was then re-equilibrated before the compression test was also trialled. Here the re-equilibration time was of the order of few minutes run time, but the inherited behaviour was not disrupted. The main conclusion that can be drawn from this parametric study is that the most effective approach is to use a REV as the smallest unit cell to replicate. Figure 5 summarises all the times needed to generate the DEM models (t_{gen}) in an equilibrated condition at the wanted p_0', n_0 and Z_0.

3. The PCRM and BVPs

The technological improvement of both hardware and software and the success of the DEM in simulating fundamental aspects of soil behaviour have increased the interest in applications for direct simulation of engineering scale BVPs in geotechnical applications. If quantitative results are sought, the DEM sample initialisation becomes one of the most difficult and time-consuming aspects of the numerical model. In this respect, in the following it is shown how the PCRM, which has proven to be an efficient approach to prepare REVs, can be used to efficiently initialise 2D and 3D BVP numerical models. First a general overview of the process is presented and some exemplar applications are shown. Then a detailed analysis of 3D cylindrical sample preparation to model calibration chambers (CCs) under gravity conditions is presented. CCs are used to experimentally find correlations between penetration resistance and soil state (Jamiolkowski et al., 2003). As these experiments are relatively complicated, long and require an expensive laboratory setup recently the modelling of CCs has gained more and more interest (Mcdowell et al., 2012; Zhang et al., 2018a, 2018b). One of the main difficulties in modelling CCs with DEM is sample preparation (Butlanska et al., 2009) and, as presented in section 3.2, employing the PCRM, with some precautions when dealing with the boundaries, will make sample preparation very effective and efficient.

3.1. General methodology

To illustrate the concept behind BVP generation using the PCRM and to highlight the computational efficiency of adopting this method, the PCRM is here employed to initialise a large scale 2D domain, of base B and height H, under any gravitational field g (Figure 6). The intent is to show how any stress profile can be generated through the PCRM, hence using the DEM as a virtual experimental centrifuge platform. Centrifuge lab tests are widely used in geomechanics and, by imposing an increased 'gravitational' acceleration to the physical model, it is possible to reproduce in the lab self-weight stress profiles comparable to the ones in the field. In this way, it possible to obtain accurate data to help solve complex geotechnical problems (Bolton et al., 1999; White and Lehane, 2004; Liang et al., 2017). Centrifuge tests however are expensive and time consuming, so accurate DEM models may be useful in helping to design the experiments themselves. The approach considered to initialise a 2D centrifuge DEM model is schematized in Figure 7 and can be summarised as follows.

- Generate a LxL 2D periodic cell and equilibrate a sample under a stress state such that a) the effective vertical stress (σ'_v) corresponds to the effective vertical stress the ground should have at a depth of H and b) the effective horizontal stress (σ'_h) corresponds to the target k_0.
- Replicate the cell □□times in the horizontal direction and □□times in the vertical direction.
- Loop through all the contacts and scale the CF by a ratio z/H where z is the depth from the ground level to the position of the contact.
- As described in more detail below, introduce a virtual overlap δ^g which gives the exact scaled CF from part (iii) but does not change the physical overlap δ of the particles.
- Activate gravity and fix a thin layer of particles in contact with the boundaries.
- Cycle to equilibrate.

The approach also applies for 3D problems where the initial REV is a 3D periodic cell which has to be then replicated in a third dimension. For point (iv) above the value to assign to δ^g in order to modify original contact force $F_N{}^0$ to scaled contact force $F_N{}^{scaled}$ (Figure 8) results

$$\delta^g = \frac{F_N^0 - F_N^{scaled}}{k_n} = \delta - \frac{F_N^{scaled}}{k_n} \qquad (1)$$

in case a linear contact model is used, while

$$\delta^g = \left(\frac{F_N^0}{h_n}\right)^{2/3} - \left(\frac{F_N^{scaled}}{h_n}\right)^{2/3} = \delta - \left(\frac{F_N^{scaled}}{h_n}\right)^{2/3} \qquad (2)$$

For the Hertzian contact model. In Eqs. (1) and (2), k_n and h_n represent the normal contact stiffness for the corresponding contact models respectively. The main limitation of this general approach is that the boundaries are composed by fixed particles; hence they are 'rough'. Such effect can be limited by increasing the domain size, but the difficulty of imposing zero shear stresses at the boundaries would remain.

3.2. Application of the PCRM in the presence of rigid boundaries

As already mentioned above, generating DEM models for CCs, which require the presence of rigid or flexible servo-controlled lateral boundaries, is very time consuming. In this section two approaches aimed at tacking such a limitation are proposed: Method A starts from a cubic REV cell and, using the PCRM (similarly to the general procedure presented above), fills the cylindrical domain. Method B requires the generation of an initial sample which is characterised by a rigid cylindrical wall in the radial direction and periodic boundary conditions in the cylinder axis direction.

3.2.1. Method A

Referring to Figure 9, the rigid wall cylinder sample generation can be summarised as follows.

- Generate a LxLxL 3D periodic cell and equilibrate a sample under a stress state such that a) σ'_v corresponds to the effective vertical stress the ground should have at a depth of H and b) σ'_h corresponds to target k_0.
- Replicate the cell ξ times in the x direction, ψ times in the y direction and ζ times in the vertical direction.
- Delete any particle whose centre is outside of the cylinder and below the base wall.
- Perform 1 mechanical cycle to generate the inevitable large CFs between the rigid walls and the particles in contact with them.
- Assign to the wall-particle contacts a value corresponding to the mean CF of the original REV by adjusting the contact gap (δ^g).
- Continue from step (iii) of the general methodology (section 3.1) described above without fixing particles at the boundaries.

3.2.2. Method B

This method is aimed at completely removing the rigid cylinder-wall boundary effects which are inevitable for Method A above. The concept here is to generate a thin cylindrical sample having periodic boundaries in the cylinder axis direction and a rigid cylinder in the radial one (Figure 10). By means of a servo control of the rigid cylinder and the periodic domain, it is possible to equilibrate the cylindrical REV to the required σ'_v and σ'_h (i.e. radial stress) at the

desired porosity. At this point, referring to Figure 11, the equilibrated CC model can be obtained by the following.

- Loading the 3D cylindrical - only periodic in *z* - cell up to a stress state such that a) σ'_v corresponds to the vertical stress the ground should have at a depth of H and b) the radial stress corresponds to target k_0.
- Replicating the cell ζ times in the vertical direction.
- Continuing from step (iii) of the general methodology (section 3.1) described above without fixing particles at the boundaries.

4. Results

4.1. 2D BVPs

First, the efficiency of adopting the PCRM to prepare a 2D virtual centrifuge model is presented. The geometrical dimension of the sample and the number of particles (N_p) involved to generate the model are summarised in Table 4. Both 1*g* and 10*g* samples were prepared and Figure 12 illustrates the final state of the equilibrated 2D centrifuge models. As can be observed from the distribution of porosity (n), σ'_v and σ'_h, the final samples are homogenous and the target stress profiles are captured very well. The time required to prepare the model was roughly 30 minutes. To compare the computational advantage of using the PCRM, a third sample was prepared using the Pluviation Method (PM) under 1*g* gravity conditions. The time required to equilibrate the latter resulted to be around 11,000 minutes (just over 1 week). The stress trends obtained with the PCRM and PM model are compared with the theoretical trend in Figure 13. It is clear that for the same quality of result the PCRM is really efficient compared to the PM, which is the most common method used to recreate k_0 conditions in DEM. Moreover, with the PCRM it is also possible to better control the desired k_0 conditions, which are a direct result of sedimentation in the PM.

4.2. 3D BVPs

To assess the efficiency of using the PCRM a cylindrical shaped sample (Figure 14a) is generated using two well-known methods and both Method A and B presented in the previous section, as presented in Figure 15. The two more traditional methods are the sedimentation method (SM) and a method consisting of generating a 'cloud' of non-contacting particles. In the former case, particles are generated at some height above the final analysis domain and then allowed to fall downwards under a vertical body force. This process involves significant particle movements and many collisions resulting in a varying contact configuration. Consequently, the computational cost of this stage is high. It is therefore faster to create a 'cloud' of close but non-contacting particles by employing the random number generation approach within the system domain and apply gravity to these particles, allowing them to settle. Moreover, to ensure sample homogeneity, these two existing methods were performed in 3 steps of 100 mm thickness each.

Following Arroyo et al. (2011) and similarly to Ciantia et al. (2014, 2016a), a factor of 38 is applied to increase particle sizes of FS (Figure 14b) with the aim of reducing the final number of particles filling the chamber. The contact parameters are the same as the samples presented in Section 2 (Table 2). In addition to the time required to generate each sample, the quality of the end result is gauged on final porosity and stress distributions. Figure 14c shows the cubic and cylindrical periodic REVs required for method A and B. According to the volume response analysis, the N_p in the cubic REV (3290) is comparable to the *M* sample in Section 2

which was considered to be the minimum sized REV. Assuming axisymmetric conditions, 2D contours for porosity and stresses of each of the four samples are presented in Figure 16 and Figure 17. Porosity calculations accounted for corrections needed to consider particles crossing the averaging volumes, while for the average stress calculations within each portion the individual particles' representative stresses were weighted for their own volume only when the centre is inside the averaging volume. Figure 16 represents the corresponding contours for *n*, while Figure 17 reports values for vertical, radial and circumferential stresses (σ_z, σ_r, σ_θ). The theoretical (expected/target) trends are compared with the numerical ones in Figure 18, by considering only the internal region and disregarding the boundaries. It is clear that satisfactory results, both in terms of porosity and stress state distributions, are obtained employing these two innovative methods, especially Method B. In Method A, despite the internal homogeneity, boundary effects are clearly visible. Finally, Figure 19 compares the time required to generate the samples with the different techniques and adopting the PCRM combined with Method B is clearly the most efficient and effective approach.

5. Conclusions

In this paper an original approach for fast initialisation of DEM models has been presented. The periodic cell repetition method (PCRM) builds upon a simple idea: using equilibrated periodic DEM models which are large enough to form a REV to fill larger spaces. This idea is complemented by force scaling to initialise anisotropic stress fields of magnitude variable in space. The computational efficiency, control of initial conditions and homogeneity of the generated specimen make the PCRM very attractive for simulations requiring large scale DEM models.

List of notations

α	cell-replication factor in the horizontal direction (2D mode)
β	cell-replication factor in the vertical direction (2D model)
BVP	boundary value problem
CF	contact force
C_u	homogeneity coefficient
D_{50}	median particle size
ΔD	diameter expansion coefficient
δ	physical contact overlap
δ^g	virtual contact overlap
DEM	discrete element method
ε_{vol}	volumetric strain
ε_z	axial strain
F_b	sum of the magnitudes of all the forces acting on a body b
F_N^0	original contact force
F_N^{scaled}	scaled contact force
FS	Fontainebleau sand
g	gravity acceleration
G	shear modulus
H	BVP model height
h_n	normal contact stiffness (Hertz contact model)
k_0	coefficient of earth pressure at rest
k_n	normal contact stiffness (linear contact model)
L	cell length
L	large sample
L-CRS(S)	large small-cell replicated samples
L-CRS(M)	large medium-cell replicated samples
M	medium sample
MS	measurement sphere
μ	interparticle friction coefficient
n	porosity
n_0	initial porosity
$n_{0,int}$	initial internal porosity
N_p	number of particles
ν	Poisson's ratio
p_0'	initial effective mean normal stress
PCRM	periodic cell replication method
PM	pluviation method
ψ	cell-replication factor in the y direction (3D model)
PSD	particle size distribution
q	deviatoric stress
ρ	radial coordinate
ρ_s	grain density
REM	radius expansion method
REV	representative elementary volume
S	small sample
S^*	small sample with higher initial coordination number
SM	sedimentation method

σ_h' horizontal effective stress
σ_θ' circumferential effective stress
σ_v' vertical effective stress
σ_z' longitudinal stress
t_{gen} sample generation time
U_b magnitude of the unbalanced force acting on a body b
v_{ini} initial velocity
ξ cell-replication factor in the x direction (3D model)
y* vertical axis downward from free surface in 2D BVPs
Z coordination number
Z_0 initial coordination number
$Z_{0,int}$ initial internal coordination number
ζ cell-replication factor in the z direction (3D model)

References

Agnolin, I., Roux, J.-N., 2007a. Internal states of model isotropic granular packings. I. Assembling process, geometry and contact networks.

Agnolin, I., Roux, J.-N., 2007b. Internal states of model isotropic granular packings. III. Elastic properties. Phys. Rev. E 76, 61304.

Arroyo, M., Butlanska, J., Gens, A., Calvetti, F., Jamiolkowski, M., 2011. Cone penetration tests in a virtual calibration chamber. Géotechnique 61, 525–531.

Bolton, M.D., Gui, M.W., Garnier, J., Corte, J.F., Bagge, G., Laue, J., Renzi, R., 1999. Centrifuge cone penetration tests in sand. Géotechnique 49, 543–552.

Butlanska, J., Arroyo, M., Gens, A., 2009. Homogeneity and Symmetry in DEM Models of Cone Penetration. AIP Conf. Proc 425–428.

Butlanska, J., Arroyo, M., Gens, A., O'Sullivan, C., 2014. Multi-scale analysis of cone penetration test (CPT) in a virtual calibration chamber. Can. Geotech. J. 51, 51–66.

Calvetti, F., 2008. Discrete modelling of granular materials and geotechnical problems. Eur. J. Environ. Civ. Eng. 12, 951–965.

Calvetti, F., Tamagnini, C., Viggiani, G., 2003. Micromechanical inspection of constitutive modelling. In: Hevelius (Ed.), Constitutive Modelling and Analysis of Boundary Value Problems in Geotechnical Engineering. Benevento, pp. 187–216.

Cheung, G., O'Sullivan, C., 2008. Effective simulation of flexible lateral boundaries in two- and three-dimensional DEM simulations. Particuology 6, 483–500.

Ciantia, M., Arroyo, M., O'Sullivan, C., Gens, A., Liu, T., 2018. Grading evolution and critical state in a discrete numerical model of Fontainebleau sand. Géotechnique.

Ciantia, M., Arroyo, M., Zhang, N., Emam, S., 2017. Periodic cells for large-scale problem initialisation. In: EPJ Web of Conferences.

Ciantia, M.O., Arroyo, M., Butlanska, J., Gens, A., 2016a. DEM modelling of cone penetration tests in a double-porosity crushable granular material. Comput. Geotech. 73, 109–127.

Ciantia, M.O., Arroyo, M., Butlanska, J., Gens, a., 2014. DEM modelling of a double porosity crushable granular material. Proc. Int. Symp. Geomech. from Micro to Macro 269–274.

Ciantia, M.O., Arroyo, M., Calvetti, F., Gens, A., 2015. An approach to enhance efficiency of dem modelling of soils with crushable grains. Geotechnique 65.

Ciantia, M.O., Arroyo, M., Calvetti, F., Gens, A., 2016b. A numerical investigation of the incremental behavior of crushable granular soils. Int. J. Numer. Anal. Methods Geomech. 40, 1773–1798.
Ciantia, M.O., Arroyo, M., Gens, A., Calvetti, F., 2014. Particle failure in DEM models of crushable soil response. In: Hicks, M.A., Brinkgreve, R.B.J., Rohe, A. (Eds.), Numerical Methods in Geotechnical Engineering. CRC Press/Balkema, Leiden, the Netherlands, pp. 345–350.
Ciantia, M.O., Shire, T., 2017. An efficient large-scale DEM model initialisation procedure. In: Proceedings of the 25th UKACM Conference on Computational Mechanics. p. 13.
Cundall, P.A., Strack, O.D.L., 1979. A discrete numerical model for granular assemblies. Géotechnique 29, 47–65.
Esnault, V.P.B., Roux, J.-N., 2013. 3D numerical simulation study of quasistatic grinding process on a model granular material. Mech. Mater. 66, 88–109.
Huang, X., Hanley, K.J., O'Sullivan, C., Kwok, F.C.Y., 2014a. Effect of sample size on the response of DEM samples with a realistic grading. Particuology 15, 107–115.
Huang, X., O'Sullivan, C., Hanley, K.J., Kwok, C.Y., 2014b. Discrete-element method analysis of the state parameter. Géotechnique 64, 954–965.
Itasca, C.G.I., 2017. PFC — Particle Flow Code, Ver. 5.0.
Jamiolkowski, M., Lo Presti, D.C.F., Manassero, M., 2003. Evaluation of Relative Density and Shear Strength of Sands from CPT and DMT. In: Soil Behavior and Soft Ground Construction. American Society of Civil Engineers, Reston, VA, pp. 201–238.
Jiang, M.J., Konrad, J.M., Leroueil, S., 2003. An efficient technique for generating homogeneous specimens for DEM studies. Comput. Geotech. 30, 579–597.
Katsuki, S., Ishikawa, N., Ohira, Y., Suzuki, H., 1989. Shear strength of rod material. J. Civ. Eng. 410, 1–12.
Kuhn, M.R., 1995. A flexible boundary for three- dimensional dem particle assemblies. Eng. Comput. 12, 175–183.
Liang, T., Knappett, J.A., Bengough, A.G., Ke, Y.X., 2017. Small-scale modelling of plant root systems using 3D printing, with applications to investigate the role of vegetation on earthquake-induced landslides. Landslides 14, 1747–1765.
Mcdowell, G.R., Falagush, O., Yu, H.-S., 2012. A particle refinement method for simulating DEM of cone penetration testing in granular materials. Géotechnique Lett. 2, 141–147.
Rothenburg, L., Bathurst, R.J., 1992. Micromechanical features of granular assemblies with planar elliptical particles. Géotechnique 42, 79–95.
Roux, J.-N., 2004. Internal state of granular assemblies near random close packing.
Seif El Dine, B., Dupla, J.C., Frank, R., Canou, J., Kazan, Y., 2010. Mechanical characterisation of matrix coarse-grained soils with a large-sized triaxial device. Can. Geotech. J. 47, 425–438.
Tamagnini, C., Calvetti, F., Viggiani, G., 2005. An assessment of plasticity theories for modeling the incrementally nonlinear behavior of granular soils. J. Eng. Math. 52, 265–291.
Thornton, C., 2000. Numerical simulations of deviatoric shear deformation of granular media. Géotechnique 50, 43–53.
Thornton, C., Zhang, L., 2010. On the evolution of stress and microstructure during general 3D deviatoric straining of granular media. Géotechnique 60, 333–341.
Ting, J.M., Corkum, B.T., Kauffman, C.R., Greco, C., 1989. Discrete Numerical Model for Soil Mechanics. J. Geotech. Eng. 115, 379–398.

White, D.J., Lehane, B.M., 2004. Friction fatigue on displacement piles in sand. Géotechnique 54, 645–658.
Zhang, N., Arroyo, M., Ciantia, M., Gens, A., 2018a. DEM Investigation of Particle Crushing Effects on Static and Dynamic Penetration Tests. In: Wu, W., Yu, H.-S. (Eds.), Proceedings of China-Europe Conference on Geotechnical Engineering. Springer, Cham, Vienna, pp. 274–278.
Zhang, N., Arroyo, M., Gens, A., Ciantia, M., 2018b. DEM modelling of dynamic penetration in granular material. In: Cardoso, A.S., Gomes, A.T., Costa, P.A., Marques, J.C., Vierira, C. (Eds.), Proceedings of the 9th European Conference on Numerical Methods in Geotechnical Engineering (NUMGE). Taylor & Francis Group London, UK, Porto, p. 415/418.

Table 1.

Sample	p_0' [kPa]	$n_{0,int}$ [-]	n_0 [-]	$Z_{0,int}$ [-]	Z_0 [-]	N_p [-]	t_{gen} [min]
S	10	0.373	0.376	2.84	2.53	1,465	4
M	10	0.375	0.387	2.37	2.30	5,036	31
L	10	0.378	0.388	2.43	2.34	40,326	160
*S**	10	0.372	0.376	3.45	3.23	1,465	4

Table 2.

μ [-]	G [GPa]	ν [-]	D_{50} [mm]	C_u [-]
0.275	3	0.3	0.21	1.57

Table 3.

Sample	p_0' [kPa]	$n_{0,int}$ [-]	n_0 [-]	$Z_{0,int}$ [-]	Z_0 [-]	N_p [-]	t_{gen} [min]
L-CRS(S)	10	0.379	0.377	2.51	2.53	39,555	4+8
L-CRS (M)	10	0.387	0.387	2.74	2.44	40,288	31+6
L-CRS (S) ΔD	10	0.378	0.376	2.42	2.35	39,555	4+8+60

Table 4.

H [m]	B [m]	Number of disks per cell [-]	Total number of disks [-]
1.1	1	2,511	45,910

Figure captions

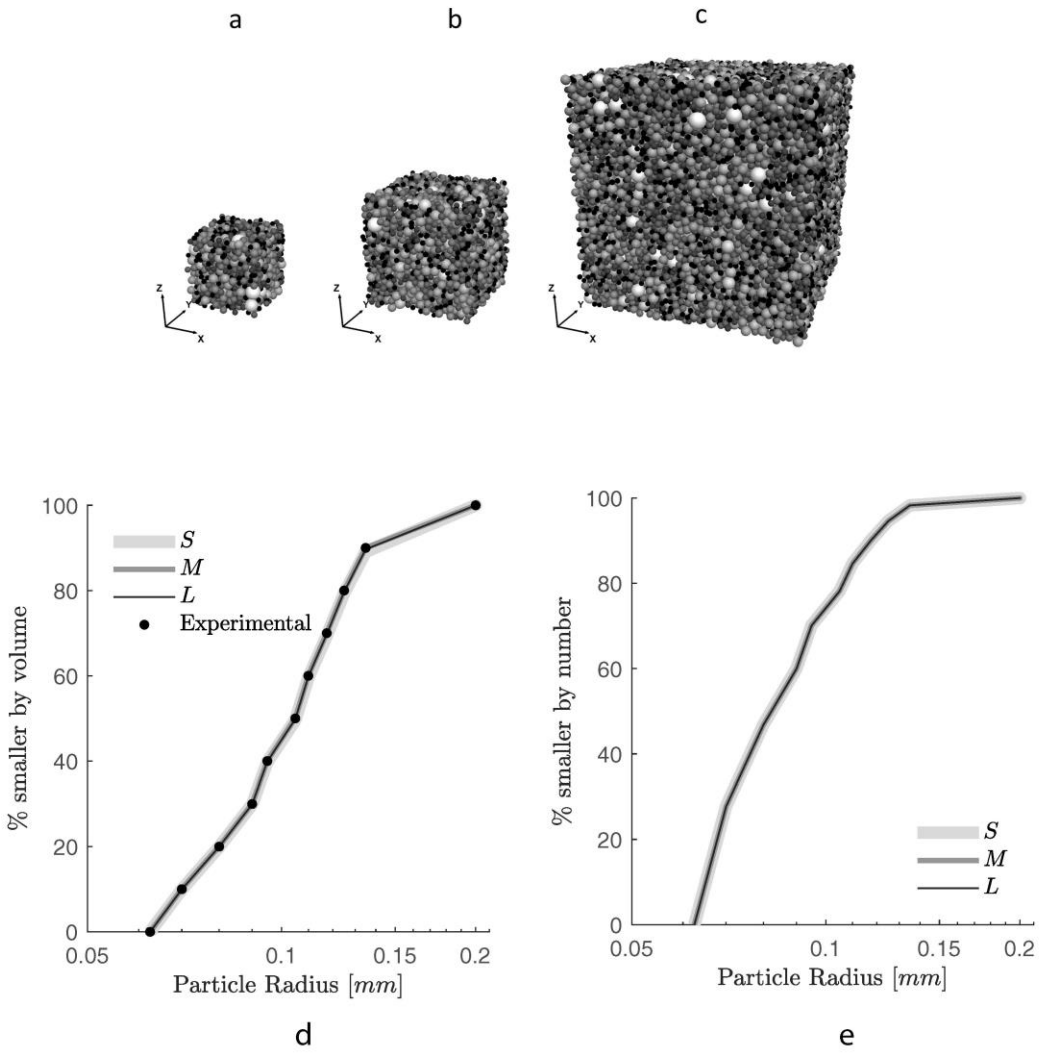
a
b
c
z
y
x
100
80
60
40
20
0
0.05
0.1
0.15
0.2
S
M
L
Experimental
% smaller by volume
Particle Radius [mm]
d
% smaller by number
Particle Radius [mm]
e

Figure 1

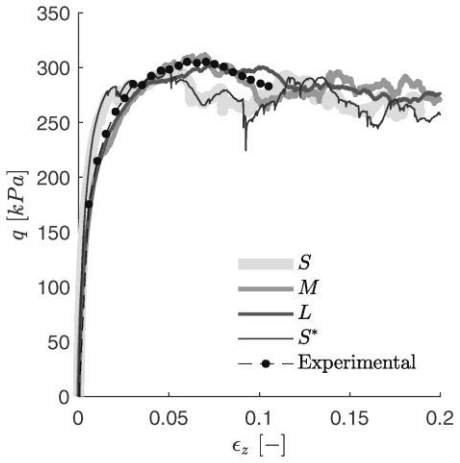
350
300
250
200
150
100
50
0
$q\ [kPa]$
0
0.05
0.1
0.15
0.2
$\epsilon_z\ [-]$
S
M
L
S^*
Experimental

a

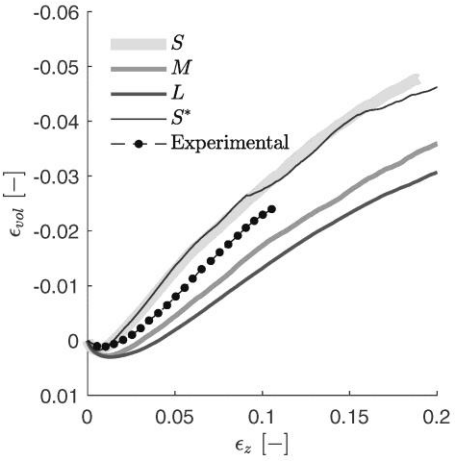
-0.06
-0.05
-0.04
-0.03
-0.02
-0.01
0
0.01
$\epsilon_{vol}\ [-]$
0
0.05
0.1
0.15
0.2
$\epsilon_z\ [-]$
S
M
L
S^*
Experimental

b

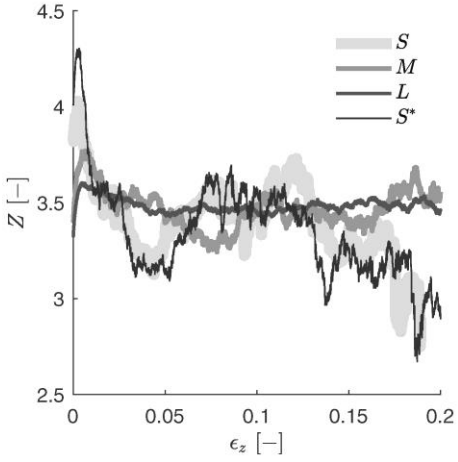
4.5
4
3.5
3
2.5
$Z\ [-]$
0
0.05
0.1
0.15
0.2
$\epsilon_z\ [-]$
S
M
L
S^*

c

Figure 2

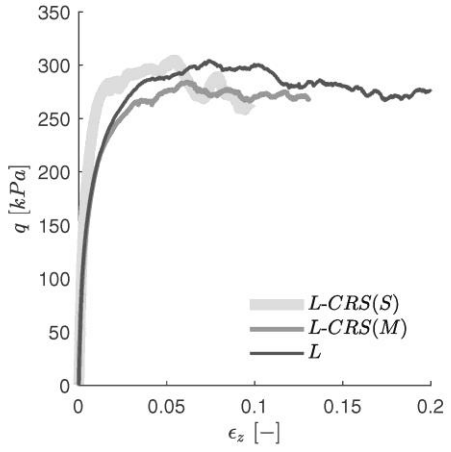
350
300
250
200
150
100
50
0
$q\ [kPa]$
0
0.05
0.1
0.15
0.2
$\epsilon_z\ [-]$
L-CRS(S)
L-CRS(M)
L

a

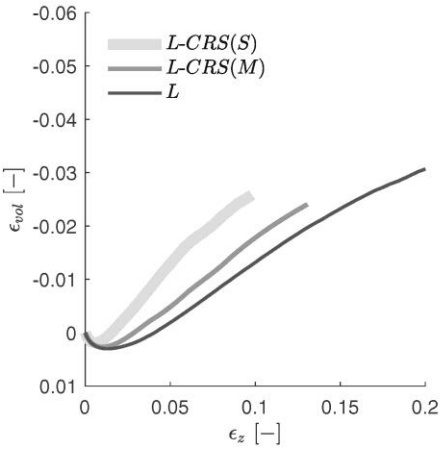
-0.06
-0.05
-0.04
-0.03
-0.02
-0.01
0
0.01
$\epsilon_{vol}\ [-]$
0
0.05
0.1
0.15
0.2
$\epsilon_z\ [-]$
L-CRS(S)
L-CRS(M)
L

b

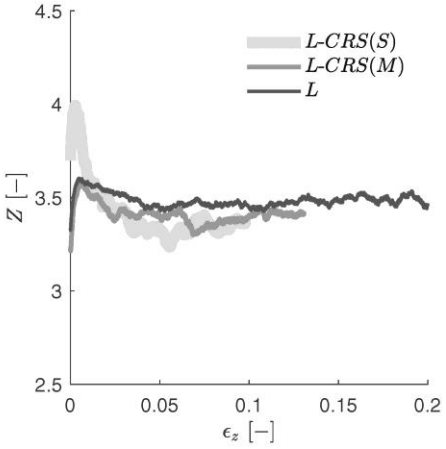
4.5
4
3.5
3
2.5
$Z\ [-]$
0
0.05
0.1
0.15
0.2
$\epsilon_z\ [-]$
L-CRS(S)
L-CRS(M)
L

c

Figure 3

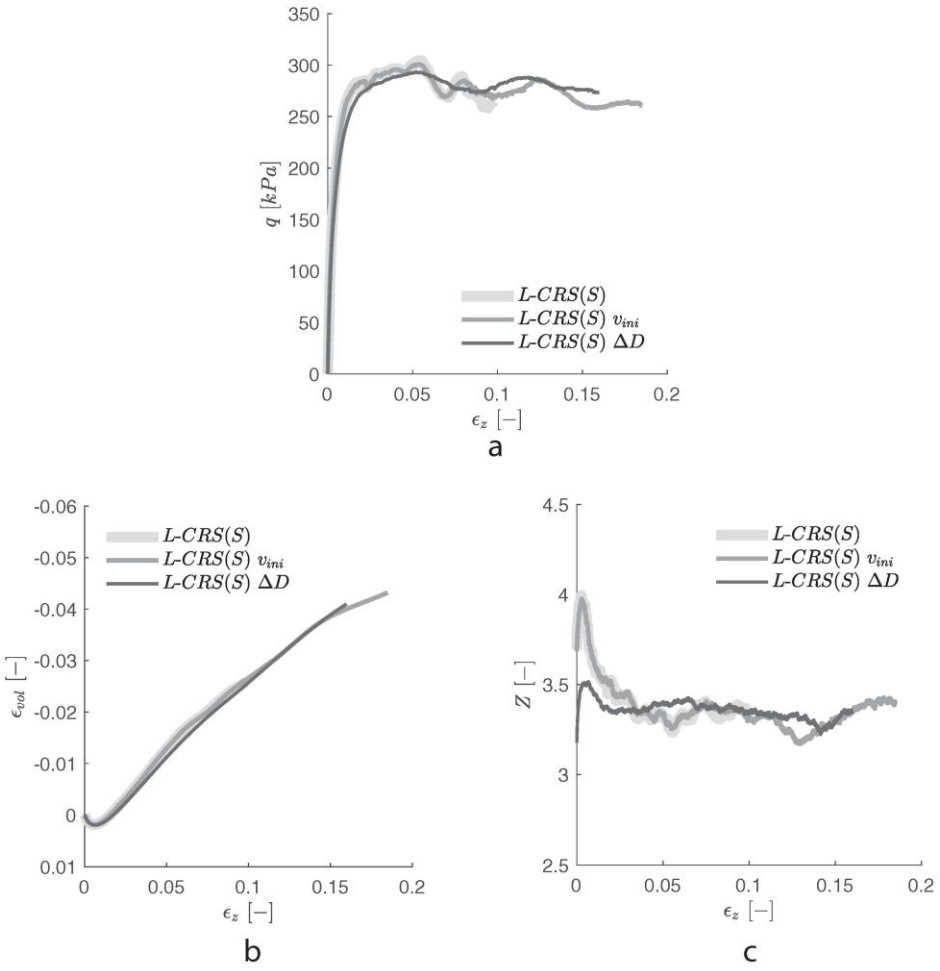
350
300
250
200
150
100
50
0
q [kPa]
0
0.05
0.1
0.15
0.2
ϵ_z [−]
L-CRS(S)
L-CRS(S) v_{ini}
L-CRS(S) ΔD
a
-0.06
-0.05
-0.04
-0.03
-0.02
-0.01
0
0.01
ϵ_{vol} [−]
ϵ_z [−]
b
4.5
4
3.5
3
2.5
Z [−]
ϵ_z [−]
c

Figure 4

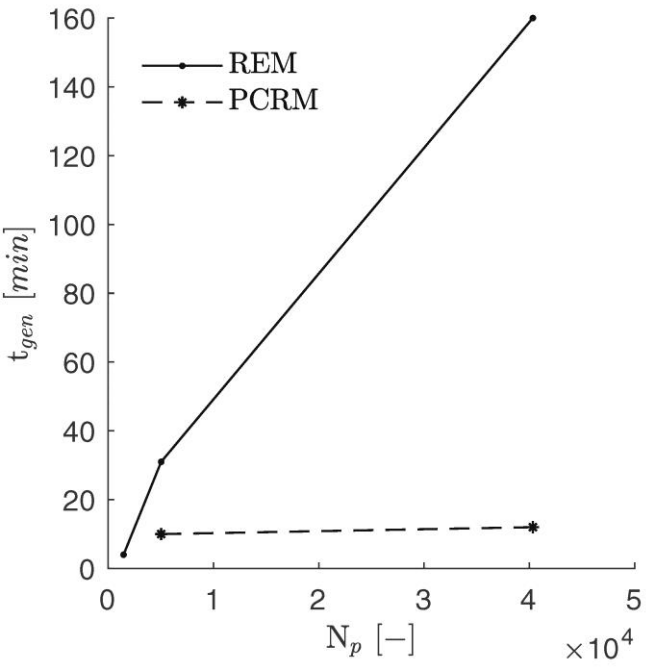
160
140
120
100
80
60
40
20
0
REM
PCRM
t_{gen} $[min]$
0
1
2
3
4
5
N_p $[-]$
$\times 10^4$

Figure 5

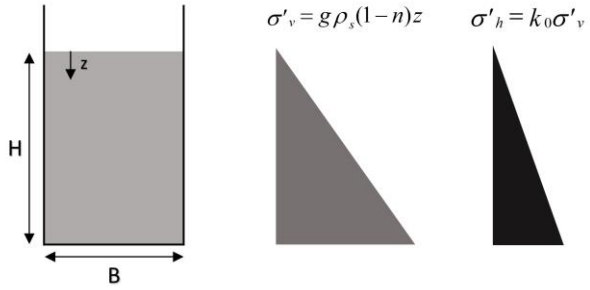

Figure 6

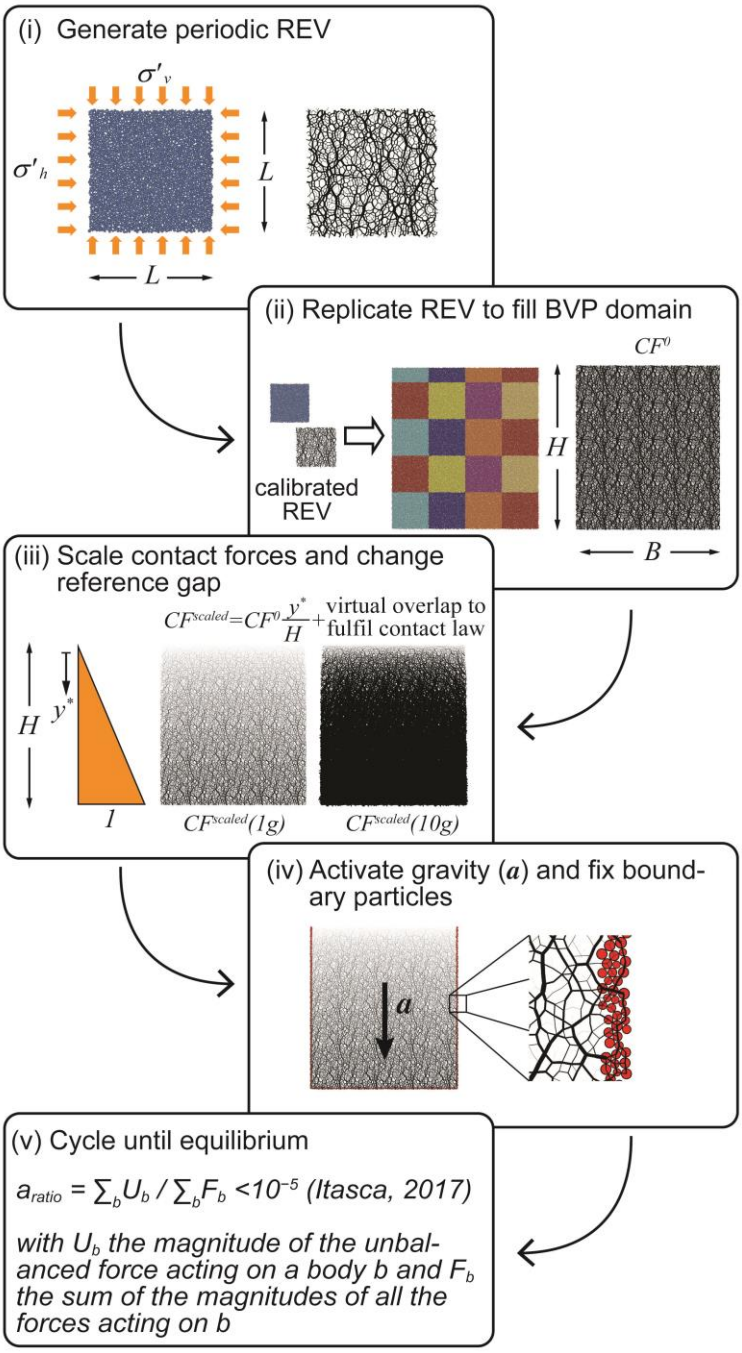
(i) Generate periodic REV
σ'_v
σ'_h
L
L
(ii) Replicate REV to fill BVP domain
CF^0
calibrated REV
H
B
(iii) Scale contact forces and change reference gap
$CF^{scaled}=CF^0\frac{y^*}{H}+$ virtual overlap to fulfil contact law
H
y^*
1
$CF^{scaled}(1g)$
$CF^{scaled}(10g)$
(iv) Activate gravity ($\boldsymbol{a}$) and fix boundary particles
$\boldsymbol{a}$
(v) Cycle until equilibrium
$a_{ratio} = \sum_b U_b / \sum_b F_b < 10^{-5}$ (Itasca, 2017)
with U_b the magnitude of the unbalanced force acting on a body b and F_b the sum of the magnitudes of all the forces acting on b

Figure 7

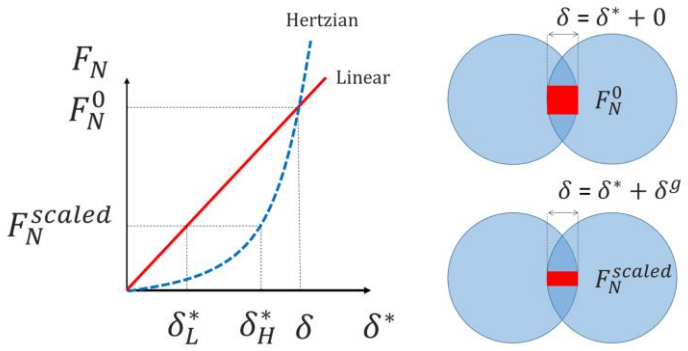
Hertzian
Linear
F_N
F_N^0
F_N^{scaled}
δ_L^*
δ_H^*
δ
δ^*
$\delta = \delta^* + 0$
F_N^0
$\delta = \delta^* + \delta^g$
F_N^{scaled}

Figure 8

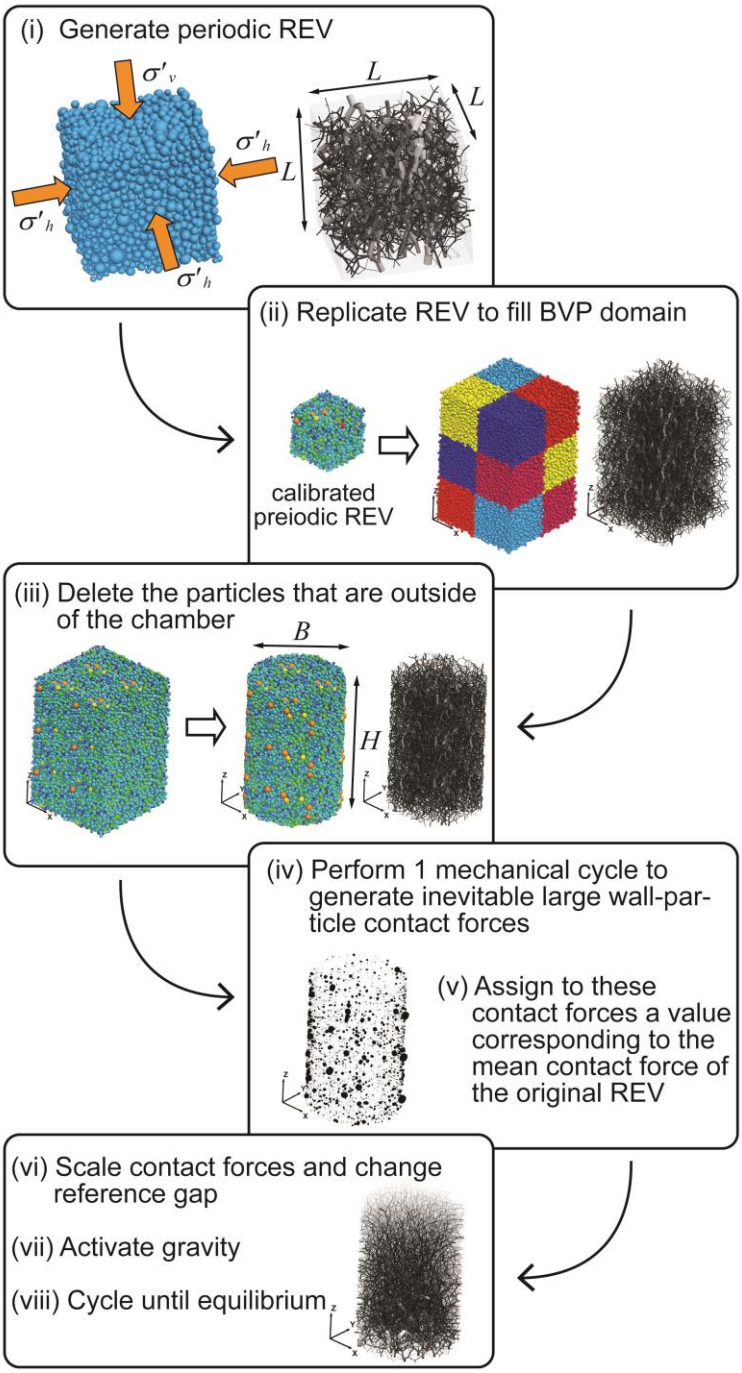
(i) Generate periodic REV
σ'v
σ'h
σ'h
σ'h
L
L
L
(ii) Replicate REV to fill BVP domain
calibrated
preiodic REV
(iii) Delete the particles that are outside of the chamber
B
H
(iv) Perform 1 mechanical cycle to generate inevitable large wall-particle contact forces
(v) Assign to these contact forces a value corresponding to the mean contact force of the original REV
(vi) Scale contact forces and change reference gap
(vii) Activate gravity
(viii) Cycle until equilibrium

Figure 9

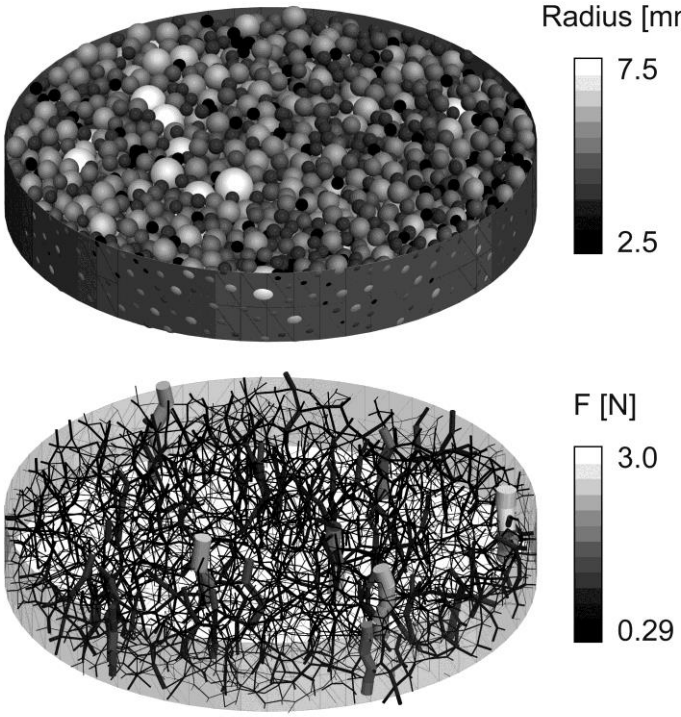

Figure 10

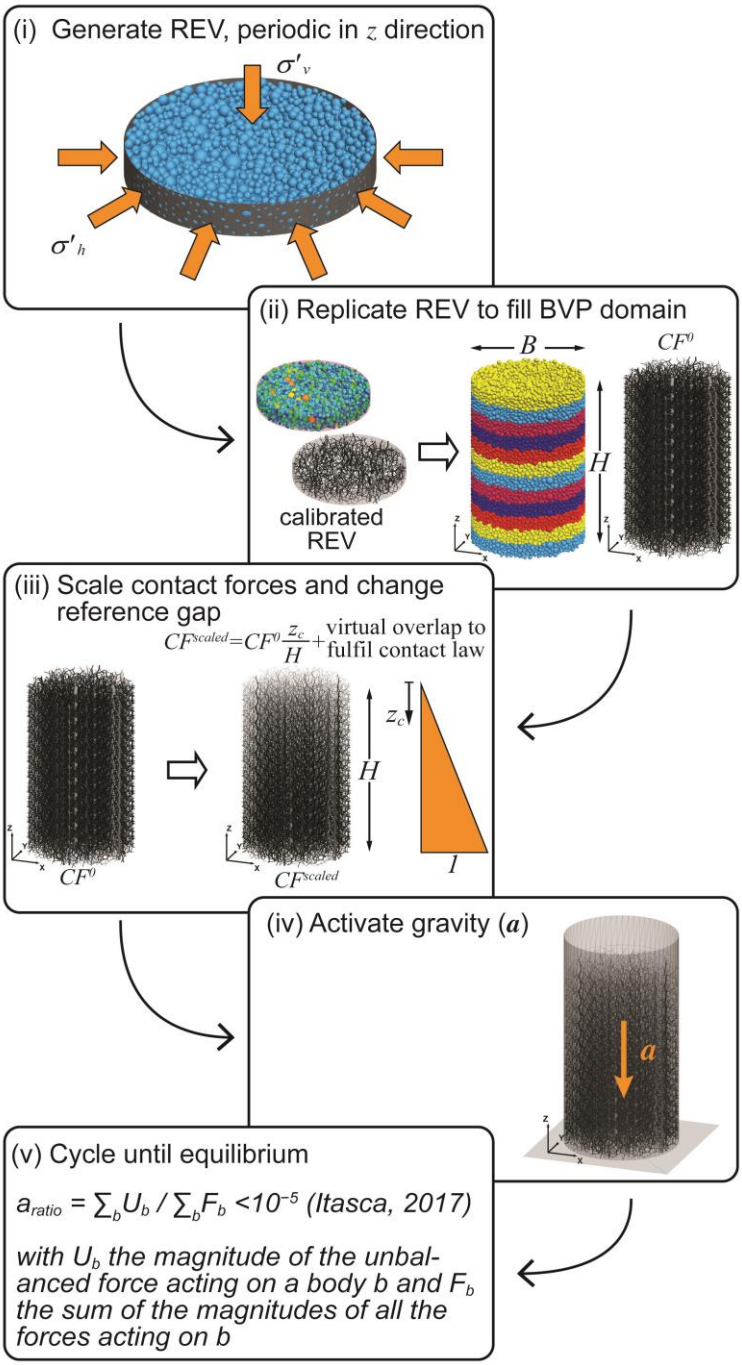
(i) Generate REV, periodic in z direction
σ'v
σ'h
(ii) Replicate REV to fill BVP domain
B
CF0
H
calibrated REV
(iii) Scale contact forces and change reference gap
CFscaled=CF0 zc/H + virtual overlap to fulfil contact law
zc
H
1
CF0
CFscaled
(iv) Activate gravity (a)
a
(v) Cycle until equilibrium
aratio = ∑b Ub / ∑b Fb <10−5 (Itasca, 2017)
with Ub the magnitude of the unbalanced force acting on a body b and Fb the sum of the magnitudes of all the forces acting on b

Figure_11

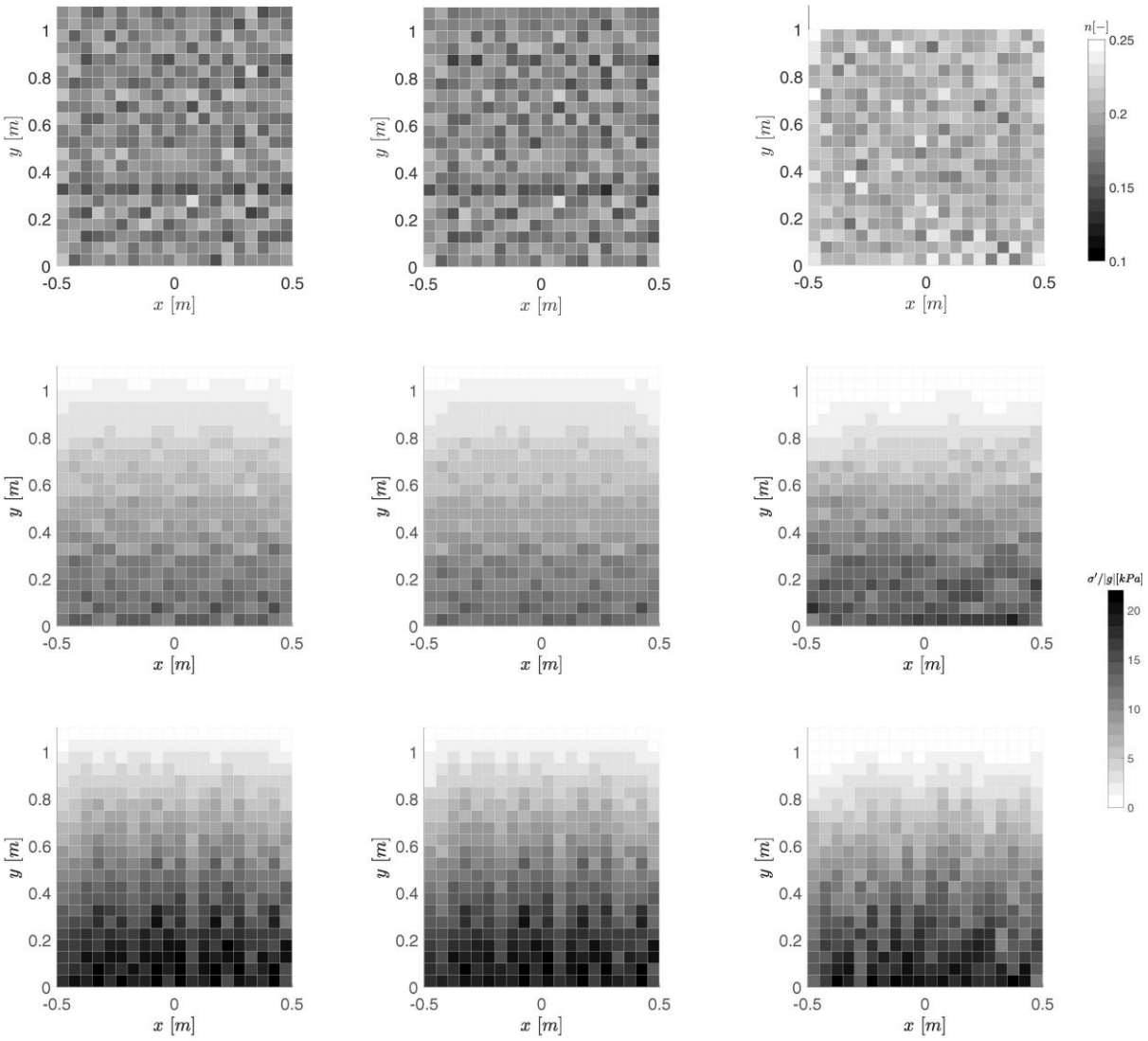

Figure 12

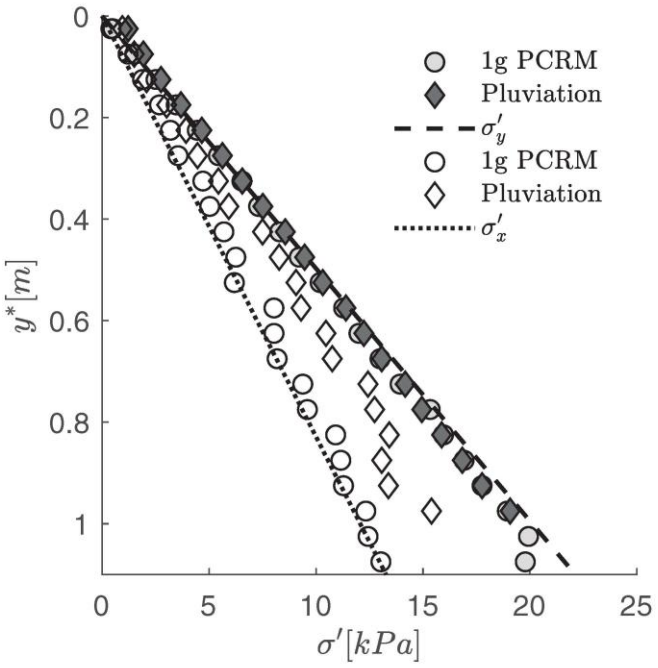
0
0.2
0.4
0.6
0.8
1
$y^*[m]$
0
5
10
15
20
25
$\sigma'[kPa]$
1g PCRM
Pluviation
σ'_y
1g PCRM
Pluviation
σ'_x

Figure 13

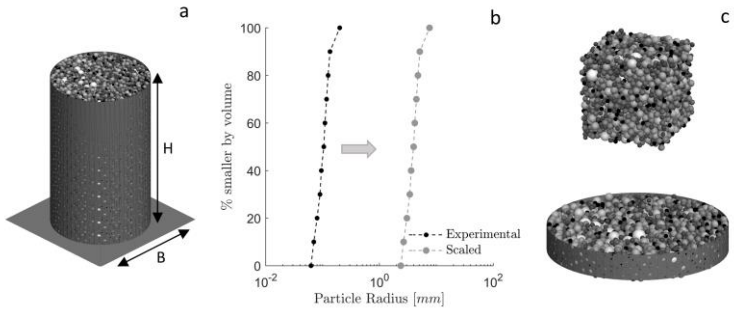
a
H
B
b
% smaller by volume
100
80
60
40
20
0
10^{-2}
10^{0}
10^{2}
Particle Radius [mm]
Experimental
Scaled
c

Figure 14

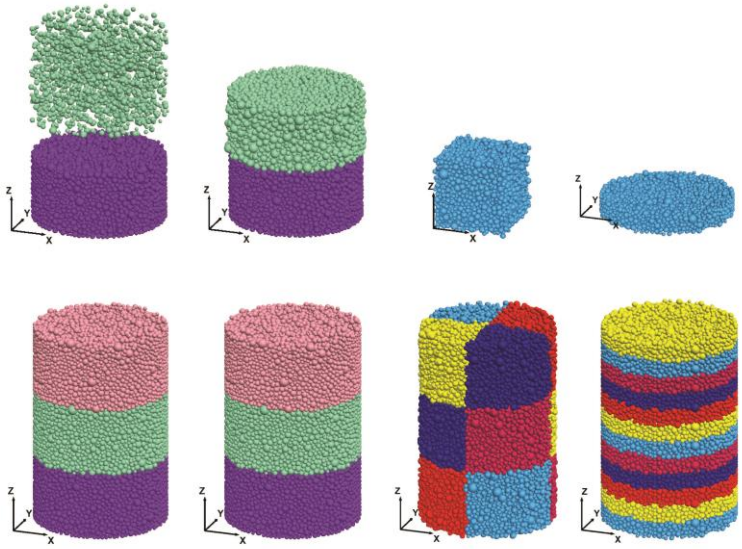

(N_p = 30,793)
a) Sedimentation

(N_p = 29,486)
b) Non-contacting particles cloud

(N_p = 29,504)
c) PCRM Method A

(N_p = 31,770)
d) PCRM Method B

Figure 15

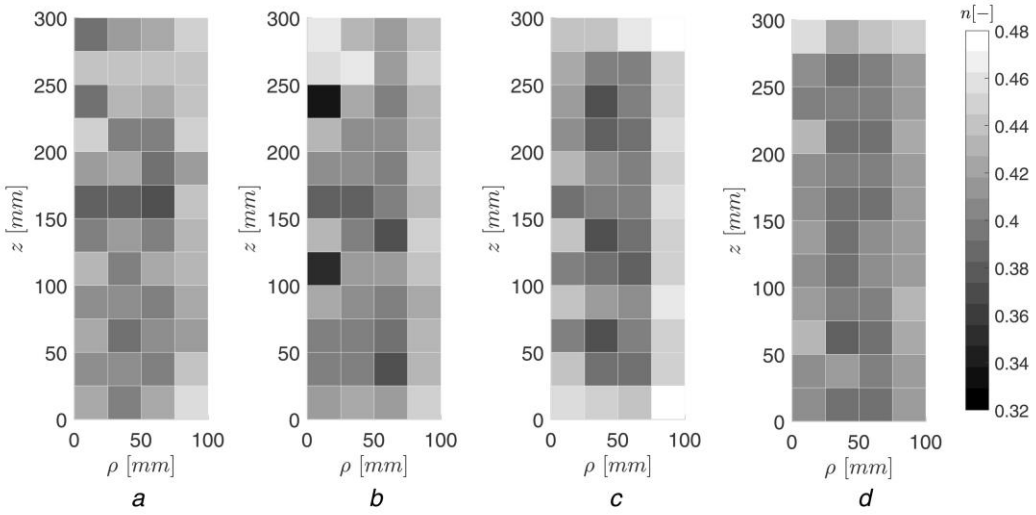
300
250
200
150
100
50
0
$z\ [mm]$
0
50
100
$\rho\ [mm]$
a
b
c
d
$n[-]$
0.48
0.46
0.44
0.42
0.4
0.38
0.36
0.34
0.32

Figure 16

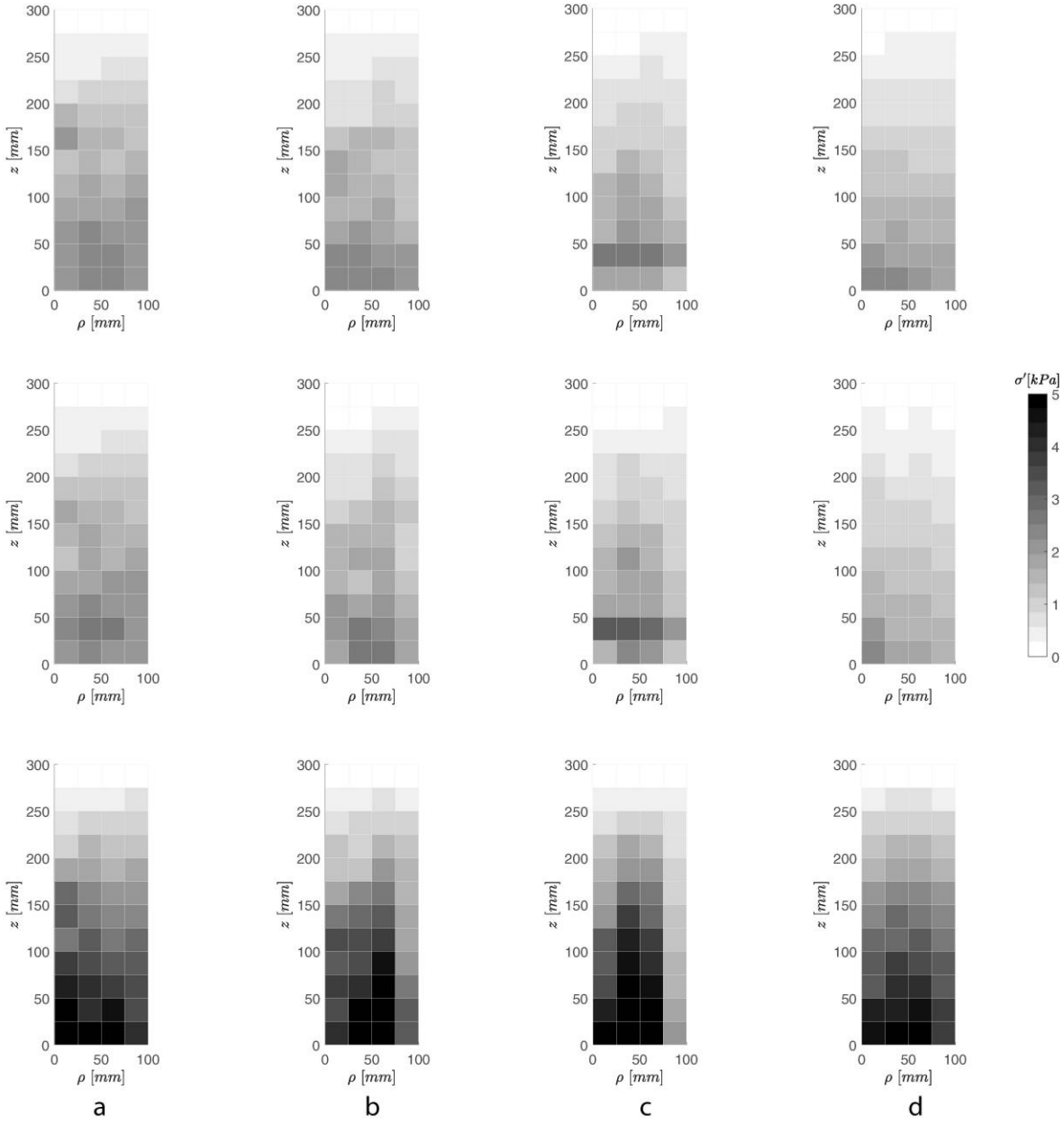

Figure 17

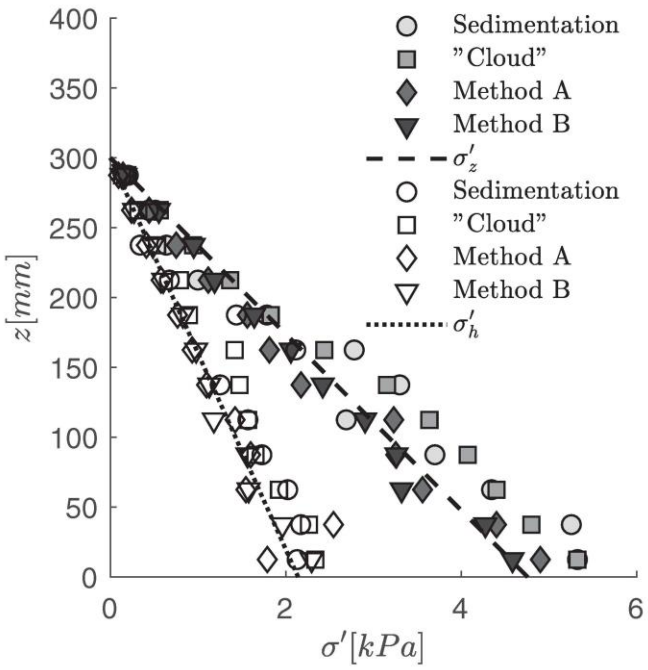
400
350
300
250
200
150
100
50
0
0
2
4
6
$z[mm]$
$\sigma'[kPa]$
Sedimentation
"Cloud"
Method A
Method B
σ'_z
Sedimentation
"Cloud"
Method A
Method B
σ'_h

Figure 18

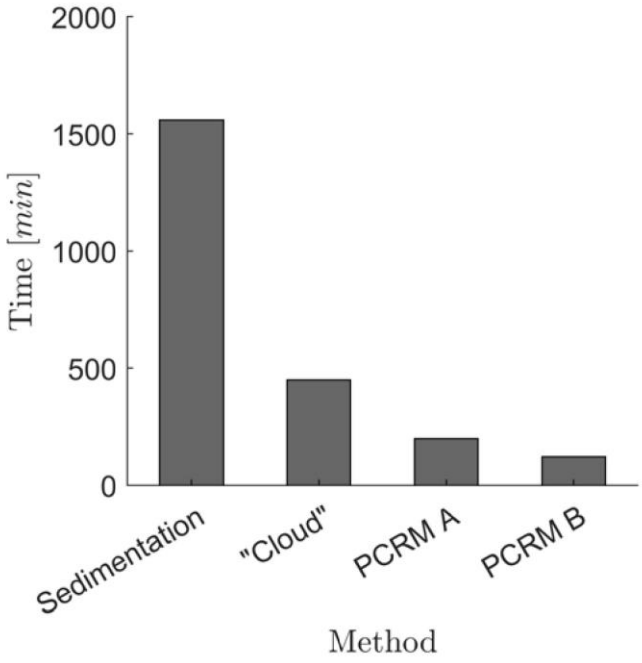
2000
1500
1000
500
0
Time [min]
Sedimentation
"Cloud"
PCRM A
PCRM B
Method

Figure 19